Laser powder bed fusion applied to the manufacture of bulk or structured magnetic cores

Valérie Baco-Carles, Thomas Huguet, Jean-François Llibre, Vincent Baylac, Isabelle Pasquet, Philippe Tailhades

Available online at www.sciencedirect.com

jmr&t Journal of Materials Research and Technology

journal homepage: www.elsevier.com/locate/jmrt

Original Article

Laser powder bed fusion applied to the manufacture of bulk or structured magnetic cores

Valérie Baco-Carles [a], *Thomas Huguet* [b], *Jean-François Llibre* [b], *Vincent Baylac* [a], *Isabelle Pasquet* [a], *Philippe Tailhades* [a,*]

[a] *UMR CNRS 5085 Cirimat, Institut Carnot Chimie Balard Cirimat, Université Toulouse III Paul Sabatier, 118 Route de Narbonne, 31 062, Toulouse Cedex 9, France*

[b] *UMR CNRS 5213 LAPLACE, Institut National Polytechnique de Toulouse, 2 Rue Charles Camichel, BP 7122, 31071, Toulouse Cedex 7, France*

ARTICLE INFO

Article history:
Received 21 January 2022
Accepted 23 February 2022
Available online 26 February 2022

Keywords:
Additive manufacturing
Laser powder bed fusion
Electric machines
Soft magnetic materials
Iron losses
Magnetic domains

ABSTRACT

Rings based on pure iron have been manufactured by laser powder bed fusion. Different experimental conditions have been implemented to manufacture simple rings called "bulk". Selected conditions were used to fabricate "structured" rings, made up of stacking of lamellae separated by weakly densified metal zones or by spacers. The magnetic properties of these rings were measured in order to determine their maximum flux density, their permeability and their magnetic losses. These properties, as well as the organizations of the magnetic domains observed by Magnetic Force Microscopy, were compared with those obtained for rings machined from castings parts or spark plasma sintered parts.

The "bulk" rings resulting from laser fusion exhibit relatively high magnetic losses of the order of 80 $W.kg^{-1}$ at 50 Hz under 1 T. However, this value can be lowered to about 30 $W.kg^{-1}$ after a SPS treatment at 750 °C. In addition to lowering the magnetic losses, SPS annealing increases the densification of the material and thus the magnetic flux. The spacing of dense metal rings by less sintered zones or by spacers ("structured rings"), makes it possible to also greatly reduce the magnetic losses. Dividing these losses by a factor of 2 is thus possible by implementing a simple geometric arrangement.

1. Introduction

Soft magnetic materials used as magnetic circuits are essential to convert electrical energy into mechanical energy and vice versa (electrical machines) or to convert electrical energy modifying the current/voltage pair (transformers). Thus, since the discovery of electromagnetic induction by Michael Faraday [1], the family of soft magnetic materials has been expanded to meet the needs of different technological applications. The properties of iron, which is the basic material of this family of metals, have been perfected by appropriate annealing, then by the addition of alloying elements such as silicon, nickel or cobalt. Specific microstructural effects in the case of amorphous or nanocrystallized metals have also been exploited. In addition, soft magnetic composites and spinel

* Corresponding author.
E-mail address: philippe.tailhades@univ-tlse3.fr (P. Tailhades).
https://doi.org/10.1016/j.jmrt.2022.02.118

ferrites have been developed to satisfy different applications, especially at high frequency. The characteristics of these materials and their preparation methods are reported in reviews or synthesis books (see for example [2–5]). Similarly, the shape of magnetic circuits made with soft magnetic parts has been improved to guide the magnetic field by reducing the various losses (hysteresis, eddy current, leakages).

The design, development and shaping of soft magnetic materials is therefore an old topic, but more relevant than ever, especially given its potential impact on environment. It is estimated that replacing the electric motors currently in service with motors using the best available technologies would indeed reduce annual CO_2 emissions by 200 billion kilograms [4]. In addition, the advent of additive manufacturing processes enhances the prospects for progress towards more efficient use of electrical energy [6]. These processes free up some machine design constraints and could also positively modify soft magnetic materials and their shaping. In addition, little material is wasted by additive manufacturing. Traditional processes, on the other hand, waste four times more material than the mass of the finished product. Their buy-to-fly ratio of 4:1 is thus significantly higher than for additive manufacturing [7]. Thus, various works have been undertaken in this direction for several years and have already led to interesting results [7,8], even if it is often considered that the additive manufacturing for the elaboration and shaping of soft magnetic materials, is still only in its infancy [9].

For metal additive manufacturing intended for electrical machines, three processes are mainly studied: Laser Powder Bed Fusion (L-PBF), Direct Energy Deposition (DED) and binder jetting. Material extrusion is also being studied, mainly for magnetic composite materials. These processes would make it possible to achieve the production of topologically optimized parts, with the aim of increasing the performance of electrical machines [6]. Their potential impact on the microstructure and 3D structuring of magnetic materials themselves, should also offer degrees of freedom. These new possibilities should lead to better trade-offs when combining the magnetic and electrical properties of materials. Magnetic parts produced by additive manufacturing already show characteristics comparable to those obtained by traditional processes [6]. Moreover, additive manufacturing is particularly relevant for brittle materials such as Fe-(≥3%) Si, which is difficult to manufacture with traditional techniques [10].

Nevertheless, the magnetic parts produced by additive manufacturing have a major disadvantage compared to conventional parts obtained with a stack of laminated metallic sheets: they allow bigger eddy current to pass and therefore have higher losses. To overcome this issue, different techniques have been studied. First, less conductive metallic alloys have been printed such as Fe-Si [10,11], Fe-Ni [12,13] and Fe–Co alloys [14,15] mostly with L-PBF technique. Then, another strategy studied is to reproduce the conventional stack of conductive and non-conductive layers thanks to specific L-PBF machines with two powder tanks [16,17]. By this way, the combination of 300μm-thick iron and iron aluminum alloy laminae, which have low electrical conductivity, thus allows to reduce losses from 4.7 $W.kg^{-1}$ to 0.5 $W.kg^{-1}$, under a field of 0.2 T at a frequency of 50 Hz [16]. A similar approach has been followed to form lamellar structures from iron and silicon [17]. In this case, however, the reduction of eddy current losses could not be observed, because of inter-diffusion of iron and silicon and a resulting strong change in magnetic and electrical properties. Still in order to reduce the magnetic losses, other strategies were followed. They consisted in structuring the metallic materials by taking advantage of the versatility of additive manufacturing. Slits parallel or perpendicular to the construction plane of the parts were thus created to reduce eddy currents [16]. Parts composed of iron-silicon alloy laminae separated by spacers or complex shapes with Hilbert structures at the laminae interfaces have also been fabricated [18]. Significant reductions in induced current losses have thus been achieved, highlighting the value of additive manufacturing.

Surprisingly, pure iron has so far been little studied for L-PBF processing for electrical machines. Pure iron has higher magnetic properties than the commonly studied Fe–Si, Fe–Ni and some Fe–Co alloys, but has higher electrical conductivity, which implies higher eddy current losses. Pure iron has the collateral advantage of not containing carcinogenic [19], expensive, critical and strategic elements such as Co or Ni. Various works relating to the production of parts by L-PBF have however been carried out in order to study the densification processes and the mechanical properties [20–25]. Parts with relative densities between 74% and 99% of the powder density could thus be obtained with powders from different processes.

The present work is devoted to the study of the magnetic performance of different pure iron rings. Its first objective is to evaluate the effects of the L-PBF technique on the magnetic properties of "bulk" iron parts. Comparisons are thus made with reference iron rings, but obtained by more conventional techniques (conventional metallurgy or spark plasma sintering). Some possibilities offered by additive manufacturing are also exploited to "structure" the iron rings and reach the second objective of the work presented. The aim is to evaluate the reduction of magnetic losses induced by the structuring of pure iron parts and to assess the prospects of application to electrical machines free of toxic elements or with high economic criticality. Rings made of alternating dense and porous layers or dense layers separated by spacers are therefore fabricated to progress in this direction.

To try to understand the origin of the evolution of the magnetic properties of the parts (magnetic volume flux, relative permeability, magnetic losses) according to the manufacturing mode or conditions, all the samples are also characterized by various techniques (chemical analysis, electronic or magnetic microscopy, X-ray diffraction and density measurements).

2. Experimental

2.1. *Analytical techniques*

The crystalline structure of the samples was studied using Bruker AXS D4 Endeavor diffractometer equipped with a 1D LynxEye detector. Kα radiations ($\lambda K\alpha_1 = 0.15405$ nm and $\lambda K\alpha_2 = 0.15443$ nm) emitted by a copper anode, were used as X-ray source. The Kβ ray was eliminated by a nickel filter.

The microstructure of the samples was observed by scanning electron microscope (Vega3 from Tescan). The chemical

composition was analyzed by Energy Dispersive Spectroscopy (EDS) with an Oxford Instrument electron microscope analyzer. Sample cuts were made with a wire saw in order to observe the core of the samples. Magnetic Force Microscopy (MFM) observations were also done using a D3000 Digital Instrument microscope, on mirror polished samples. Magnetic tips were used at frequencies close to 65 kHz and lift scan heights of 100 nm.

A vibrating sample magnetometer VSM Quantum Design Versalab, was used to plot the hysteresis loop of samples at room temperature for directions of the applied field, perpendicular or parallel to the construction plane of the parts. Very small samples of 1–50 mg were analysed by this technique. Magnetic properties of metallic rings with a thickness of less than 7 mm and having inner and outer diameters of 55 and 65 mm respectively, were also measured by a BROCKHAUS measuring instrument type MPG 100D in accordance with the standards DIN 50 462, IEC 404–3, ISO ASTM. The ring under investigation is subjected to a magnetic field strength *H* generated by the current flowing in the primary winding. The magnetic material reacts to this field and produces a magnetic polarization *J*. This field is determined thanks to the voltage it induces in a secondary winding. The current in the primary winding is controlled so as to generate a sinusoidal B in the material as required by the standard DIN No. 50 462. The frequency domain studied varied from 3 to 2 kHz and the maximum applied magnetic field strength was 20 k.A. m^{-1}.

2.2. *Additive manufacturing by L-PBF - sintering by spark plasma sintering - solid iron machining*

The powder used for additive manufacturing and Spark Plasma Sintering (SPS) is a Goodfellow atomized iron powder with a purity greater than 99% wt. %. X-ray diffraction reveals only the presence of alpha iron (Fig. 1). No trace of iron oxide is detected. The lattice constant measured is 0.28669 ± 4.10^{-5} nm, close to the value of 0.28664 nm given in JCPDS N°06–0696. Its particle size distribution is such that the values of d10, d50 and d90 are equal to 25, 43 and 72 μm respectively. The electron micrograph and Energy Dispersive Spectroscopy (EDS) analysis of the powder are also shown in Fig. 1. No impurities were detected by EDS. The grain density measured by helium pycnometry is 7.86 $g.cm^{-3}$. The magnetization of the powder under 1592 $kA.m^{-1}$ (20 kOe) at room temperature is 217 $A.m^2.kg^{-1}$ (217 $emu.g^{-1}$). Elementary chemical analyses shown that the powder contained only 0.08% of carbon and 0.025% of nitrogen.

A 3D Systems ProX200 type laser fusion machine on a powder bed, was implemented. The 1070 nm laser beam emitted by this machine is focused in the form of a gaussian spot of 75 μm, on a work plate of 140 × 140 mm^2. The optical absorbance at this wavelength, of the iron powder used, is closed to 60%. Its power can be regulated between 30 and 300 W by step of 3 W. The experiments were carried out on powder bed thickness of 50 μm under argon gas with less than 1500 ppm of oxygen. Among the parts resulting from this process, rings with an internal diameter of 55 mm and an external diameter of 65 mm, the thickness of which was close to 7 mm, were manufactured with a view to magnetic characterizations. The real diameters of the rings after manufacturing were 54.3 ± 0.2 mm and 65.2 ± 0.2 mm.

A reference ring, called REF1, was obtained by machining an 80 mm diameter disc resulting from the SPS of the same iron powder than the one used in the L-PBF process. The SPS process was implemented under vacuum (residual pressure 10 Pa) by applying a mechanical pressure of 40 MPa and heating at 25 °C.min^{-1} to a maximum temperature of 750 °C for 10 min. Another reference ring, called REF2, was obtained by machining in a commercial iron bar (purity higher than 99.8 wt. %).

As an illustration, pictures of the bulk rings studied in this paper are presented in Fig. 2.

3. Results and discussion

3.1. *Bulk magnetic cores*

As mentioned in the introduction, various works have been carried out on the manufacture of parts made of pure iron by L-PBF. Relative densities greater than 95% could be obtained [24,25]. However, approaching the recommended conditions, the parts obtained with our machine and our iron powder

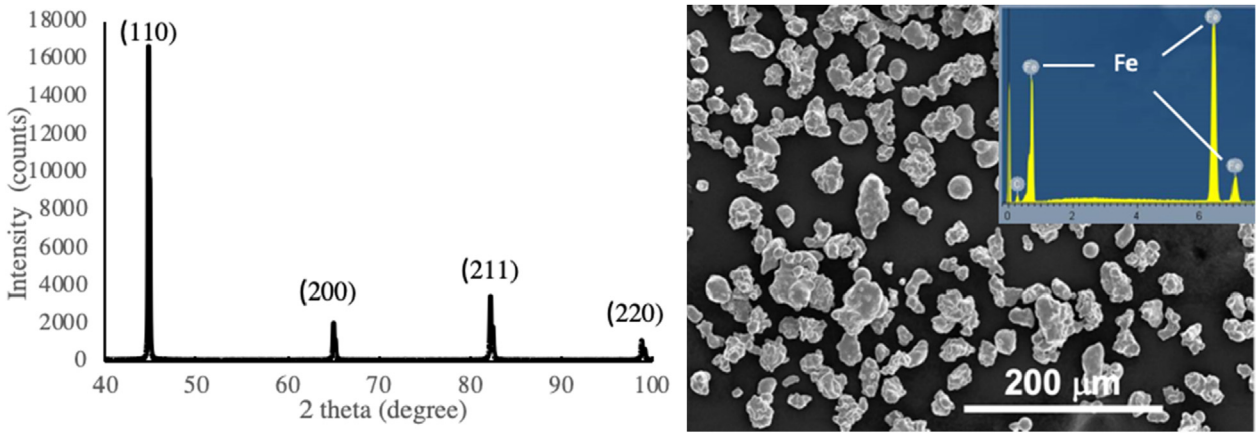

Fig. 1 – X-ray diffraction pattern, scanning electron micrograph and EDS analysis of the iron powder used for additive manufacturing and SPS.

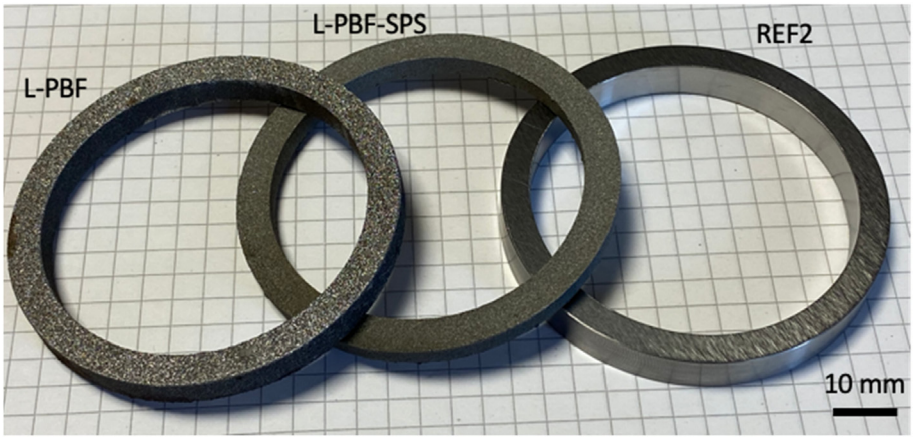

Fig. 2 – Pictures of typical bulk rings of L-PBF and L-PBF-SPS series and REF2 (see Table 1 for preparation conditions and relative densities).

gave relatively well-densified parts in the core but with arithmetic roughness higher than 50 μm (Fig. 3a).

Our goal being to manufacture parts "ready to use", i.e. well densified and not requiring machining for future use in an electric machine (Fig. 3b), we explored other manufacturing conditions. Many preliminary tests were carried out to find manufacturing conditions compatible with our objectives. The effects of three major manufacturing parameters were studied during the manufacturing of centimetric cubes. The laser power was varied from 120 to 180 W, the scanning speed from 700 to 1750 mm.s^{-1} and the spacing from 0.05 to 0.2 mm. The Fig. 4 representing the relative density of the samples as a function of the energy density of the laser per unit area (i.e. Laser power/[Laser scan speed x Hatch spacing]), allows to synthesize in a simple way, the link between the processing conditions and the densification of the samples. Figure 4 also links the relative density of the sample with their manufacturing time per unit area, which is equal to 1/[Laser scan speed x Hatch spacing].

As shown in Fig. 4, a fairly wide range of energy densities allows relative densities of the order of 65–80% to be achieved. However, the energy densities that we have chosen to fabricate the iron rings studied in this work, are of the order of 2 J.mm^{-2}. They allow us to obtain samples with densities ranging from 65% to more than 80%, with a roughness close to 50 μm for moderate manufacturing times per unit area (<0.015 s.mm^{-2}). The geometries and dimensions of the parts also conform to the computer file processed by the machine.

The experimental parameters used to fabricate the rings for electro-magnetic measurements and named L-PBF, are reported in Table 1. In this table, samples annealed by SPS are also identified and named L-PBF-SPS. This additional treatment complicates obtaining "ready-to-use" samples, since during SPS the dimensions of the samples are appreciably affected. It is also difficult to use on parts with complex shapes. However, this treatment makes it possible to densify the samples and to evaluate the importance of this parameter on the magnetic properties. It is the reason why it was carried out for some samples. The Table 1 also gathers the relative densities of the two references described in the experimental part (REF1 and REF2 were machined from a material sintered by SPS and from an iron bar, respectively).

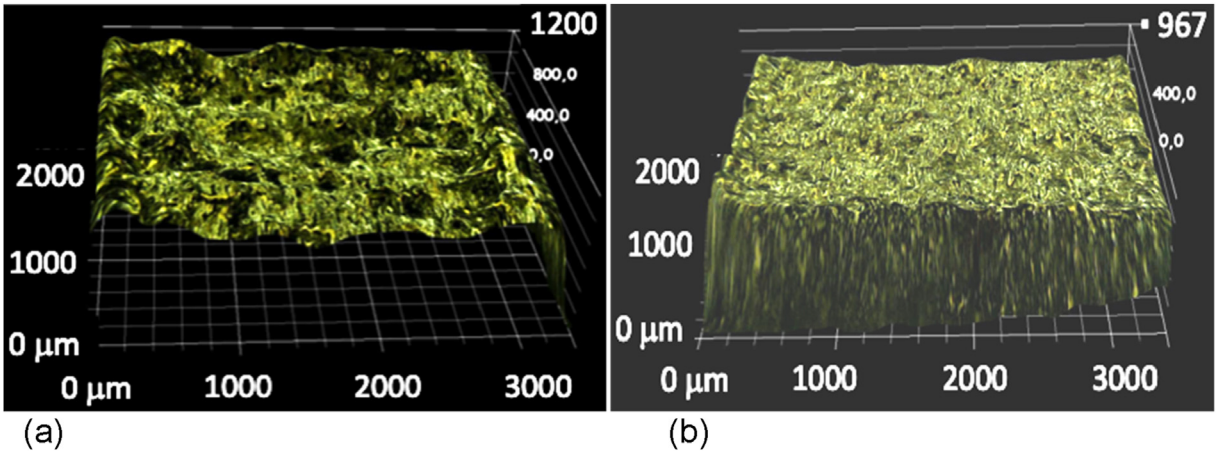

Fig. 3 – 3D optical images (a) Densified core sample with a rough surface (Ra = 60 μm); (b) Sample with a "smooth" surface" (Ra = 50 μm).

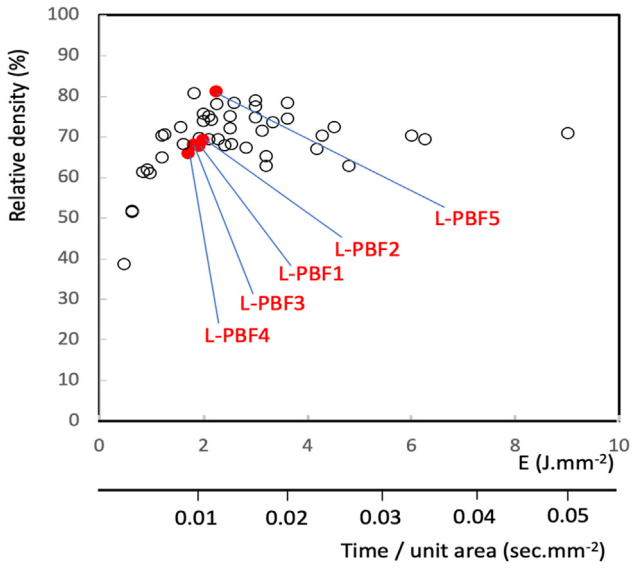

Fig. 4 – Relative density of samples as a function of their manufacturing energy density and their manufacturing time per unit area. The solid circles represent samples equivalent to the L-PBF rings studied (see Table 1).

Figure 5 shows the micrographs of the surface (Fig. 5a and b) and the cross-section of sample (Fig. 5c-d) prepared with the same conditions than L-PBF5 and L-PBF6 rings. On the surface, the microstructure is formed of contiguous parallel bands, resulting from laser scanning. Their width is approximately equal to the value of the hatch spacing. There is also the presence of a porosity and of some metallic beads resulting from powder spatters for the most part. The observation of the cross-section of the sample (Fig. 5c and d) reveals densified zones of thickness close to 5–6 μm and sparsely densified zones of thickness close to 1.5 μm, in which one can distinguish lightly sintered particles. These zones are parallel to the manufacturing plane. It is reasonable to consider that they result from the powder beds spread and then successively fused during the construction of the parts. The total thickness of the whole is however clearly lower than the 50 μm of the powder bed spread for each manufacturing plane. The densification associated with some powder projections during the laser irradiation, are responsible for this difference. The densification defects observed periodically could correspond to the lower part of each powder bed. The heat diffused in this zone after absorption of the laser energy by the surface, would indeed be insufficient to correctly fuse the powder grains. The periodic regions of low density and the porosities (Fig. 5d) which appear randomly, would lead to the relative densities of the order of 80% measured at the macroscopic scale.

X-Ray Diffraction Patterns (XRD) (Fig. 6) on centimetric samples also prepared with the same conditions than L-PBF samples set reveal that they consist of pure α-Fe. No gamma iron phase is detected, although due to the high temperatures generally reached during L-PBF [26], such a phase could be frozen by the relatively rapid cooling imposed by the process. The lattice constants of samples in the form of parallelepipeds, prepared with the same additive manufacturing parameters as the L-PBF rings are close to 0.28650 nm. These are measured parallel to the building plane of the samples. They are slightly lower than the values of 0.28664 nm given in JCPDS N°06–0696 and 0.28669 nm measured for the starting powder. A change in lattice constant was also observed for parallelepiped-shaped samples fabricated under different laser melting conditions. This change appears for samples densified to more than 65%. Depending on the manufacturing, the lattice constant is larger or smaller than that of the powder. It varies between about 0.2865 and 0.2870 nm. These variations most certainly reflect mechanical stresses of tension (low parameter) and compression (high parameter) in the manufacturing plane. Further study would be necessary to better understand the stress state of the samples as well as the link between their densification and their lattice constant.

The saturation magnetizations at room temperature (210 $emu.g^{-1}$ or 210 $A.m^2.kg^{-1}$), measured by vibrating sample magnetometer, are somewhat lower than those of the starting iron powder (217 $A.m^2.kg^{-1}$ or 217 $emu.g^{-1}$). This confirms that the resulting phase is predominantly α-Fe, although the weak magnetization could reveal the presence of a small amount of a paramagnetic γ-Fe phase not detected by XRD analysis or some non-ferromagnetic impurities present in the starting iron powder.

Measurements of magnetic flux density, relative permeability and magnetic losses were performed on the rings listed in Table 1. Although these are made of a well-known material, alpha iron, the objective was to assess the impact of the L-PBF process and the selected manufacturing parameters on its electromagnetic properties. It is indeed known that these properties can vary greatly depending on process-dependent characteristics such as relative density, microstructure,

Table 1 – Rings manufacturing parameters and relative density (powder bed thickness equal to 50 μm).

Sample	Laser Power P (W)	Scan speed v ($mm.s^{-1}$)	Hatch spacing h (mm)	Relative density (%)
L-PBF1	120	1250	0.050	67.7 ± 0.5
L-PBF2	150	1500	0.050	69.2 ± 0.5
L-PBF3	180	2000	0.050	67.9 ± 0.5
L-PBF4	150	1750	0.050	65.8 ± 0.5
L-PBF5	180	1000	0.080	83.2 ± 0.5
L-PBF6	180	1000	0.080	80.9 ± 0.5
L-PBF3-SPS1	180	2000	0.050	96.0 ± 0.5
L-PBF4-SPS2	150	1750	0.050	91.1 ± 0.5
REF1 (Machined from SPS sample)	-	-	-	89.6 ± 0.5
REF2 (Machined from iron bar)	-	-	-	99.5 ± 0.5

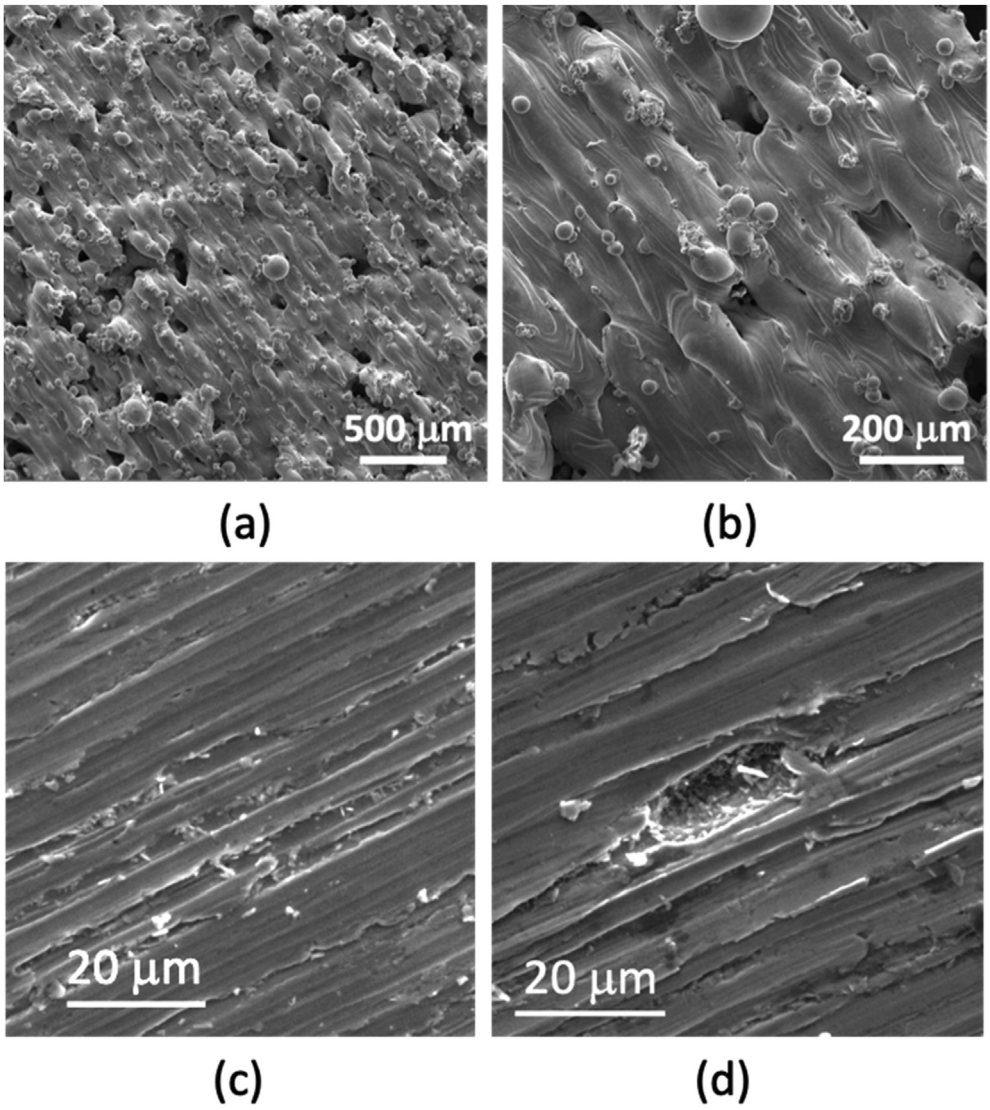

Fig. 5 – Scanning electron micrographs of a same parallelepipedal sample (10 × 10 × 5 mm^3) prepared in the same conditions than the L-PBF5 and L-PBF6 rings, with P = 180 W, v = 1000 mm s^{-1}, h = 0,08 mm and a powder bed thickness of 0.05 mm. Images of the surface (a) (b) and cross-section (c) (d). (b) is a zoom of (a), (c) and (d) are not at the same location.

mechanical stresses and structural defects. It was therefore important to compare the electromagnetic properties of the samples obtained from the L-PBF process, with those measured on the references of machined iron bar and SPS densified samples (see Experimental section and Table 1).

Some results of electromagnetic measurements are reported on Figs. 7–9. The magnetic flux density at the approach of saturation (20 kA m^{-1}; 251 Oe), logically increases with the relative density (Fig. 10). It is, however, for each additive manufactured sample, somewhat lower than that which should be achieved, if one considers that it should be equal to the product of the saturation magnetic flux density of alpha iron (2100 mT) multiplied by the relative density. This difference could reveal the presence of a small amount of γ-Fe phase even if this could not be detected by X-ray diffraction, or some non-ferromagnetic impurities, which can be revealed as small precipitates by electronic microscopy. The maximum

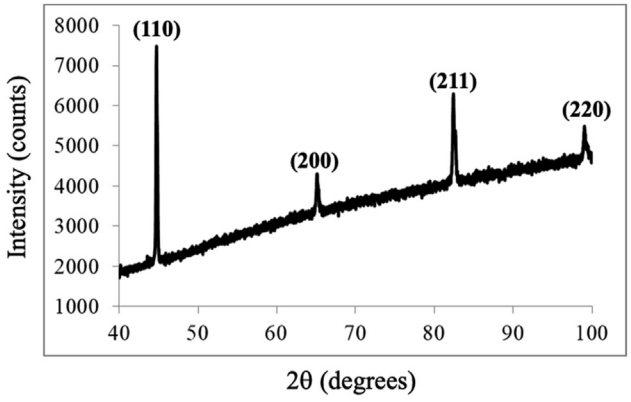

Fig. 6 – X-ray diffraction pattern of the surface of a sample prepared. with P = 180 W, v = 1000 mm.s^{-1}, h = 0.08 mm and a powder bed thickness of 0.05 mm (like L-PBF5/6).

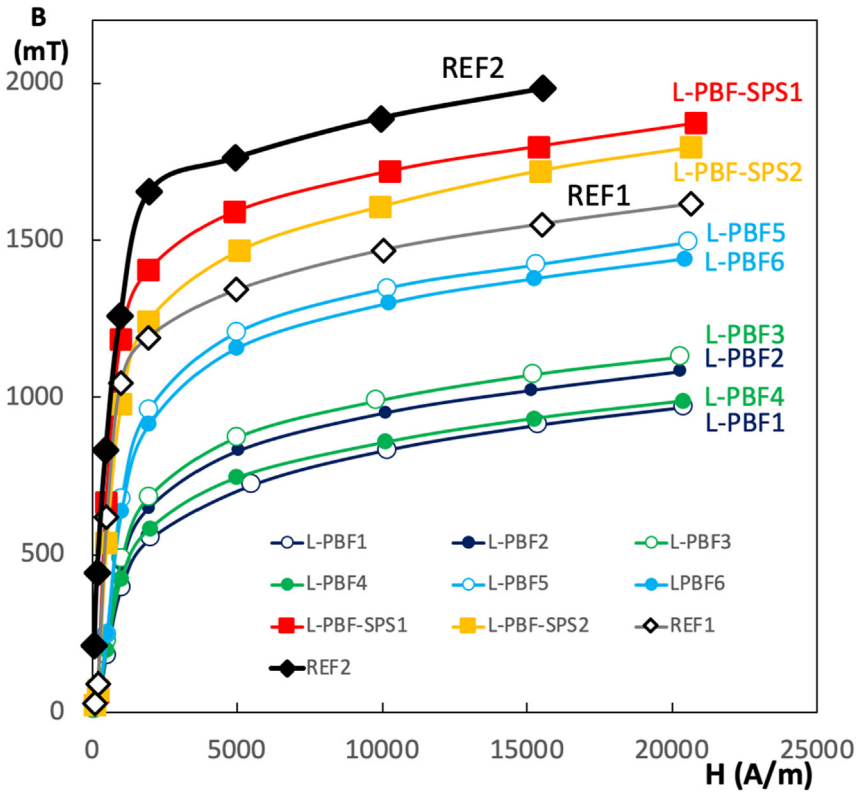

Fig. 7 – Magnetic flux density versus magnetic field strength at 20 °C. These anhysteretic magnetization curves are obtained with a low excitation frequency (3 Hz) and for various excitation amplitudes.

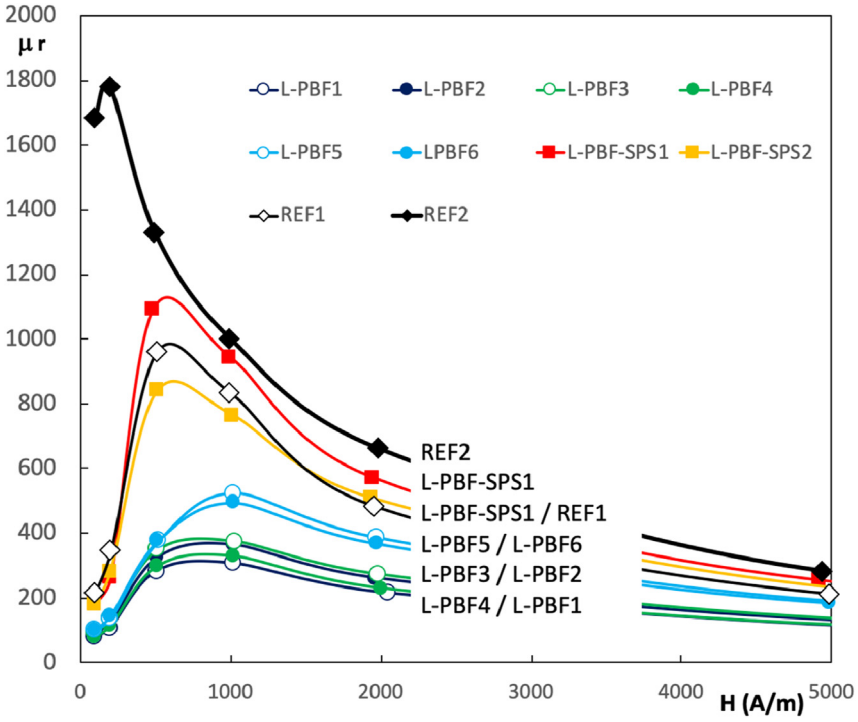

Fig. 8 – Relative permeability versus magnetic field strength. These anhysteretic magnetization curves are obtained with a low excitation frequency (3 Hz) and for various excitation amplitudes.

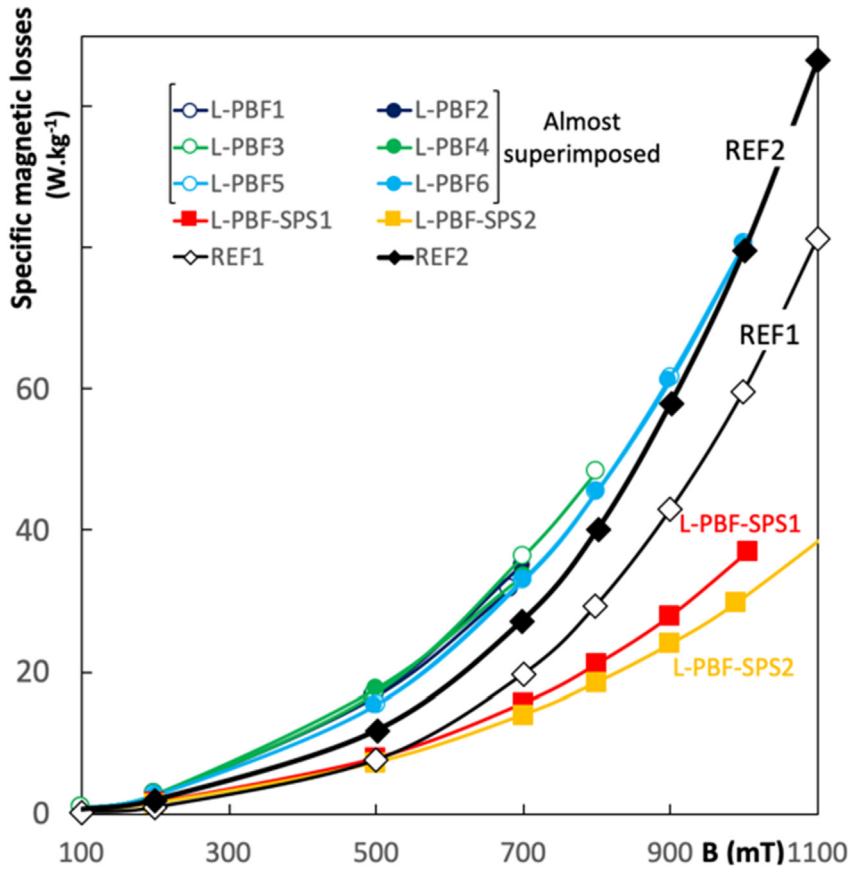

Fig. 9 – Specific magnetic losses (hysteretic + eddy current) versus magnetic flux density. The specific losses shown are obtained with a 50 Hz excitation and for various magnetic flux density amplitudes.

relative permeability is also an increasing function of relative density. The SPS-treated L-PBF samples densified to more than 90% (full squares in Fig. 10) and the reference samples (full diamonds in Fig. 10), therefore show the best B_s and $\mu_{r\,MAX}$ among the samples from the L-PBF process.

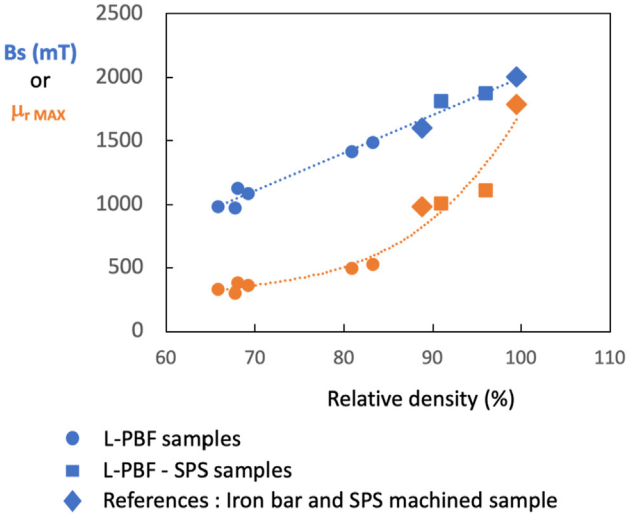

Fig. 10 – Saturation magnetic flux density B_s and maximal relative permeability μ_{rMAX} versus the relative density of the samples.

On the other hand, the influence of the relative density on the magnetic losses (Table 2) is less direct, even if for the samples L-PBF, REF1 and REF2, the latter tend to decrease slightly when the densification increases. Indeed, this trend is not observed for the LPBF-SPS samples, whose losses are significantly lower than for REF2, although their relative density is lower. These remarks apply to all the magnetic losses measured between 20 and 60 Hz, in particular for high fields of the order of 1 T, for which the experimental results are not reported in this article. Similarly, no influence of the roughness of the samples could be demonstrated.

Table 2 – Arithmetic roughness, relative density and magnetic losses for several characteristic samples.

Sample	Ra (μm)	Relative density (%)	Magnetic losses at 50 Hz and 1 T (W kg^{-1})
L-PBF3	50 ± 1	67.9 ± 0.5	78
L-PBF5	50 ± 1	83.2 ± 0.5	80
L-PBF6	50 ± 1	80.9 ± 0.5	80
L-PBF-SPS1	25 ± 1	96.0 ± 0.5	37
L-PBF-SPS2	25 ± 1	91.1 ± 0.5	31
REF1 (Machined from SPS sample)	6 ± 0.3	89.6 ± 0.5	80
REF2 (Machined from iron bar)	1 ± 0.2	99.5 ± 0.5	60

The SPS treatment of parts obtained by laser fusion therefore seems to be favorable for obtaining low-loss iron samples. The question is whether the SPS process has a specific effect or whether the reduction in losses could also be achieved by conventional annealing in an inert atmosphere, performed at the same temperature of 750 °C. A conventional annealing of this type was then performed on a sample produced under the same conditions of obtaining L-PBF6. Contrary to the SPS treatment, such a treatment does not increase the relative density but it increases very strongly the magnetic losses. At 50Hz for about 1T, they are indeed more than 5 times higher than those presented by the sample before annealing. It thus seems that the SPS treatment exerts a specific beneficial influence. This could be related to the modification of the grain boundaries and microstructure as it has been observed for different materials [27,28]. For example, SPS sintering has given higher permittivity values for barium titanates than conventional sintering techniques due to grain boundary modifications [27]. SPS has also been shown to cause chemical segregation at grain boundaries, which is on average higher than conventional sintering [28]. Therefore, the SPS annealed rings could have grain boundary and microstructure modifications, favorable for achieving low magnetic losses. In particular, impurities (<1wt%) in the iron powders, could segregate at the grain boundaries to reduce the electrical conductivity of the material as a whole and thus reduce the magnetic losses.

Finally, it appears that the L-PBF samples show high specific magnetic losses, similar or higher than the losses of the reference samples (Table 2). Only the SPS-treated L-PBF samples has losses (31 and 37W.kg^{-1}) comparable to those (36W.kg^{-1}) reported in the bibliography [16] for an iron sample obtained by additive manufacturing.

The MFM images reveal, at zero field, the magnetic domains formed in the samples. An important difference exists between the sample extracted from a foundry iron bar (REF2) and the others obtained from different production and processing routes (L-PBF, L-PBF-SPS and REF1). The REF2 sample, which also has the highest relative permeability (#1800), is indeed made up of domains that are generally very well defined and extend over large areas, although less well-organized transition zones can sometimes be found (Fig. 11). The differences between the domain structures of the other samples are not very marked. It seems, however, that the labyrinth-shaped structures, as observed in the previous reference sample, are less frequent and extensive, the lower the relative permeability of the sample. In samples of low relative permeability (# 500) a structuring into fine domains that we will qualify as "dendritic", is sometimes encountered. This structure is not observed on their counterparts having higher permeabilities. The "dendritic" structure could thus reveal microstructural defects at the origin of the fragmentation of the domains and their disorganization. The displacement of the domain walls would then be more difficult and would explain the low relative permeability. Conversely, the labyrinth-type structuring of large domains, would reveal a less faulty metal at the microstructural level and would be favorable to obtaining a high permeability.

3.2. *Structured rings*

Ferromagnetic cores, which constitute the armatures of electrical machines, are generally made of a stack of alloy sheets separated by a thin insulating layer. This type of structure, assembled piece by piece, limits the development of eddy currents, responsible for magnetic losses. In the monolithic manufacture of magnetic cores by L-PBF, it is not possible to proceed in a similar way. The main reason for this, is that commercial machines are not equipped with two different powder tanks to build multi-material parts. However, the L-PBF process offers possibilities for producing structured parts perpendicular to their construction plane. They can for example, be formed by alternately dense and porous lamellae, of the same metal. The latter will be very conductive of

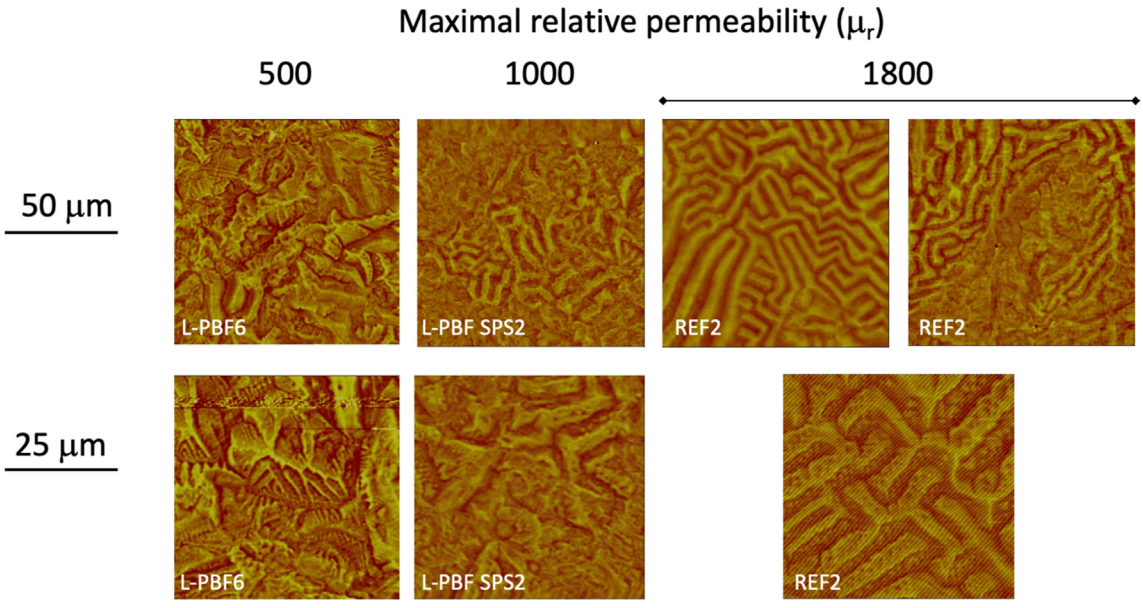

Fig. 11 – Typical magnetic domains observed by MFM for different samples having different maximal relative permeability.

Table 3 – Overall relative density, magnetic flux density, maximal relative permeability and magnetic losses for structured rings and a bulk ring manufactured with the same L-PBF parameters.

Sample	Relative density (%)	B_s Magnetic flux density at 20 kA.m^{-1} (T)	$\mu_{r\ MAX}$	Magnetic losses at 50 Hz and 1 T (W.kg^{-1})
L-PBF5	83.2	1.49	530	80
(L-PBF-structured)1 (alternation of densified and porous slats)	77.2	1.45	587	60
(L-PBF-structured)2 (superimposed slats separated by spacers)	68.4	1.25	550	42

electricity in the dense state, but much more resistive in its porous form. It is also possible to construct dense slats of section (S) separated by the thickness (e) of (n) small metallic spacers of section (s). The zone where the spacers will be located will have, in a simplified way, a total electrical resistance R such that: $R = \rho.e/(n.s)$ with ρ the metal resistivity. The electrical resistance of a dense slat of the same thickness e, on the other hand, will be

$$R_0 = \rho.e / S.$$

Consequently, R_0 will always be lower than R as soon as (n.s) will be lower than (S). It is thus possible, thanks to this type of structure, to reproduce the alternation of highly electrically conductive strips, separated by less conductive areas. In this way, an attempt can be made to reduce the magnetic losses by eddy current in a magnetic core.

Such structures have been produced in order to know their influence on the electromagnetic properties of iron cores (Table 3). The objective was to find out to what extent, this type of structuring, easily achieved by additive manufacturing, could reduce eddy current losses. Such an improvement could strongly enhance the interest for soft iron, inexpensive and environmentally friendly, in the manufacture of electrical machines.

3.2.1. *Rings formed by the alternation of densified and porous lamellae*

To obtain such structured rings, the additive manufacturing machine was set up with the previously used build parameters (P = 180 W, v = 1000 mm.s^{-1}, h = 0.08 mm, powder bed = 0.05 mm, like L-PBF5/6) to obtain the best post-lasing densities. A first annular strip 1 mm thick was thus fused. This was then covered successively with several layers of 0.05 mm of metallic powder, which was not directly exposed to the laser. On the powder bed thus formed, a second strip identical to the previous one, was built. During this operation, part of the energy supplied by the laser was naturally transferred by thermal conduction to the lower powder bed, which was thus partially sintered. In the end, the metal grains separating the two densified strips can be sufficiently sintered with each other as well as with the dense strips, to ensure a good mechanical bond. Under the manufacturing conditions used, however, this is only possible if the total thickness of the layers not directly exposed to the laser, does not exceed 0.20 mm.

The process described above was repeated to obtain the structured rings shown in Fig. 12. The thickness of the porous layers was set at 0.2 mm. This value is large enough to mark a clean microstructural transition with the densified lamellae on the one hand, and small enough to ensure good mechanical bond, on the other hand.

The measurements reveal a reduction in magnetic losses, which drop from 80 W.kg^{-1} to 60 W.kg^{-1} (Table 3) at 50 Hz and under 1 T. It is also noted that compared to the samples L-PBF5 and L-PBF6, manufactured with the same L-PBF parameters, the magnetic flux density B_s at 20 kA.m^{-1} and maximal relative permeability $\mu_{r\ MAX}$ are not strongly influenced by the structuration of the ring.

3.2.2. *Rings made up of superimposed lamellae separated by spacers*

These structured rings were constructed according to the diagram in Fig. 13. The dense slats are this time separated by spacers of circular cross-section, whose programmed diameter of which was 0.58 mm and the height of 0.6 mm. Three rows of 128 plots separate two slats. The scanning electron micrograph (Fig. 14) of a section built specifically for observation shows however, that the dimensions programmed in the machine file are not strictly observed. The dense layers are slightly thicker than their nominal value of 1 mm, in particular because of the sintering phenomenon commented above, for the first category of structured rings. The 0.6 mm spacing is therefore somewhat reduced. Furthermore, the spacers do not have perfectly constant diameters, their dimensions approaching the resolution of the process for the powder used. For this configuration, we can consider that the magnetic flux remains essentially trapped in each metal blade. Thus, there is no magnetic flux in the pads so no induced currents.

This second structure, made possible by additive manufacturing, also leads to a reduction in magnetic losses, this time from 80 W.kg^{-1} to about 42 W.kg^{-1} at 50 Hz under

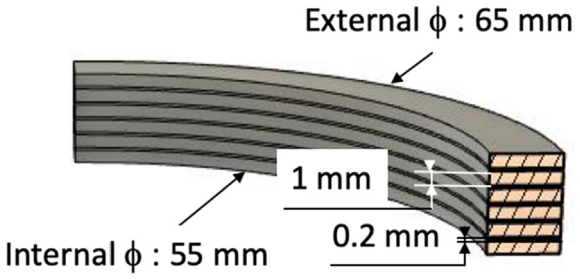

Fig. 12 – Schematic representation of a cross section of a structured quarter ring, made up of alternating dense and porous lamellae.

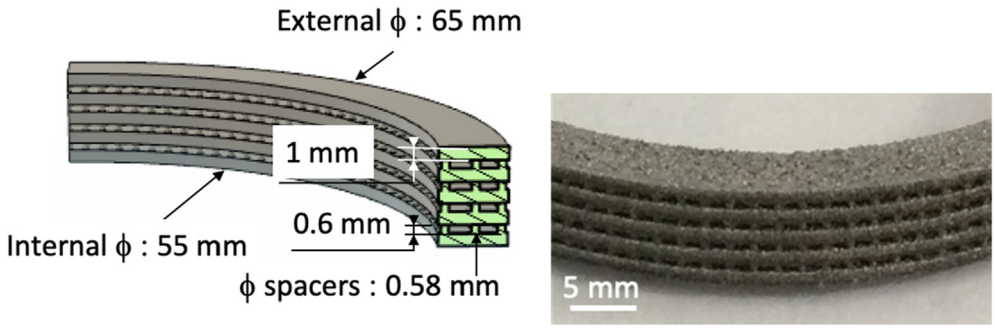

Fig. 13 – Schematic representation of a cross section of a structured quarter ring, made up of superimposed slats separated by spacers. Photography of the ring (L-PBF-structured)2.

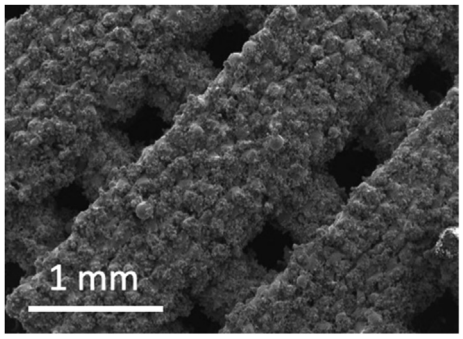

Fig. 14 – Scanning electron micrograph of a sample made up of superimposed slats separated by spacers.

1 T (Table 3). This significant reduction in magnetic losses is also achieved without strongly affecting the values of Bs and $\mu_{r\ MAX}$.

4. Conclusion

Laser powder bed fusion offers great freedom in the design of the parts, but it imposes sintering and shaping conditions on the material used, that are not necessarily favorable to obtaining the desired magnetic properties. In the case of pure iron, a material having many advantages related to its simplicity, low cost, harmlessness and recyclability, it is difficult to manufacture parts of precise geometries and very high relative densities. Very strong magnetic fluxes at saturation and high permeabilities cannot be achieved. The properties of the parts obtained directly after laser melting therefore differ significantly from those measured for their counterparts machined in a block of iron from foundry or SPS sintering. It is also noted that the magnetic domains of the laser-melted parts are smaller and much more complex in structure than for foundry iron, suggesting the existence of many microstructural defects.

The "bulk" rings resulting from laser fusion exhibit relatively high magnetic losses of the order of 80 $W.kg^{-1}$ at 50 Hz under 1 T. However, this value can be lowered to about 30 $W.kg^{-1}$ after an SPS treatment at 750 °C whose specific effect is particularly favorable to the reduction of magnetic losses. The spacing of dense metal rings by less sintered zones or by spacers, also allows to reduce strongly the magnetic losses. Dividing these losses by a factor of 2 is thus possible by implementing a simple geometric arrangement.

The dimensional optimization of the studied structures, as well as the design of new more complex structures, should allow to reduce the magnetic losses more strongly. Associated with the implementation of appropriate SPS annealing, interesting magnetic performances for technological applications could be achieved for iron cores resulting from laser powder bed fusion.

Declaration of Competing Interest

The authors declare that they have no known competing financial interests or personal relationships that could have appeared to influence the work reported in this paper.

Acknowledgements

This work was supported by grants from the French National Research Agency (ANR-21-CE05-0001-01). The authors thanks Geoffroy Chevalier for its support for Spark Plasma Sintering experiments.

REFERENCES

[1] Faraday M. Editors: R. and J.E. Taylor. Experimental researches in electricity, vol. 1. University of London; 1849 (reprinted from the Philosophical Transactions 1831-1838).
[2] O'Handley RC. Modern magnetic materials: principles and applications. John Wiley & Sons; 2000, ISBN 0-471-15566-7. p. 357–90. Chap. 10.
[3] Du Trémolet de Lacheisserie E. Magnetisme: II Matériaux et Applications. EDP Science Chap 2000;16:89–154. 2.86883.464.7.
[4] Silveyra JM, Ferrara E, Huber DL, Monson TC. Soft magnetic materials for a sustainable and electrified world. Science 2018;362:418. https://doi.org/10.1126/science.aao0195.
[5] Périgo EA, Weidenfeller B, Kollár P, Füzer J. Past, present, and future of soft magnetic composites. Appl Phys Rev 2018;5(3). https://doi.org/10.1063/1.5027045.
[6] Pham T, Kwon P, Foster S. Additive manufacturing and topology optimization of magnetic materials for electrical

machines - a review. Energies 2021;14:283. https://doi.org/10.3390/en14020283. 2021.
[7] Lamichhane TN, Sethuraman L, Dalagan A, Wang H, Keller J, Paranthaman MP. Additive manufacturing of soft magnets for electrical machine. A review Mater Today Phys. 2020;15:100255. https://doi.org/10.1016/j.mtphys.2020.100255.
[8] Périgo EA, Jacimovic J, García Ferré F, Scherf LM. Additive manufacturing of magnetic materials. Addit. Manuf. 2019;30:100870. https://doi.org/10.1016/j.addma.2019.100870.
[9] Chaudhary V, Mantri SA, Ramanujan RV, Banerjee R. Additive manufacturing of magnetic materials. Prog Mater Sci 2020;114:100688. https://doi.org/10.1016/j.pmatsci.2020.100688.
[10] Garibaldi M, Ashcroft I, Simonelli M, Hague R. Metallurgy of high-silicon steel parts produced using Selective Laser Melting. Acta Mater 2016;110:207–16. https://doi.org/10.1016/j.actamat.2016.03.037.
[11] Garibaldi M, Ashcroft I, Hillier N, Harmon S, Hague R. Relationship between laser energy input, microstructures and magnetic properties of selective laser melted Fe 6.9%wt Si soft magnets. Mater Char 2018;143:144–51. https://doi.org/10.1016/j.matchar.2018.01.016.
[12] Zhang B, Fenineche NE, Liao H, Coddet C. Magnetic properties of in-situ synthesized FeNi3 by selective laser melting Fe-80%Ni powders. J Magn Magn Mater 2013;336:49–54. https://doi.org/10.1016/j.jmmm.2013.02.014.
[13] Mikler C, Chaudhary V, Soni V, Gwalani B, Ramanujan R, Banerjee R. Tuning the phase stability and magnetic properties of laser additively processed Fe-30at%Ni soft magnetic alloys. Mater Lett 2017;199:88–92. https://doi.org/10.1016/j.matlet.2017.04.054.
[14] Yang X, Cui X, Jin G, Liu J, Chen Y, Liu Z. Soft magnetic property of (Fe60Co35Ni5)78 Si6B12Cu1Mo3 alloys by laser additive manufacturing. J Magn Magn Mater 2018;466:75–80. https://doi.org/10.1016/j.jmmm.2018.06.085.
[15] Babuska TF, Johnson KL, Verdonik T, Subia SR, Krick BA, Susan DF, et al. An additive manufacturing design approach to achieving high strength and ductility in traditionally brittle alloys via laser powder bed fusion. Addit Manuf 2020:101187. https://doi.org/10.1016/j.addma.2020.101187.
[16] Goll D, Schuller D, Martinek G, Kunert T, Schurr J, Sinz C, et al. Additive manufacturing of soft magnetic materials and components. Addit Manuf 2019;27:428–39. https://doi.org/10.1016/j.addma.2019.02.021.
[17] Kocsis B, Fekete I, Varga LK. Metallographic and magnetic analysis of direct laser sintered soft magnetic composites. J Magn Magn Mater 2020;501:166425. https://doi.org/10.1016/j.jmmm.2020.166425.
[18] Plotkowski A, Pries J, List F, Nandwana P, Stump B, Carver K, et al. Influence of scan pattern and geometry on the microstructure and soft magnetic performance of additively manufactured Fe-Si Addit. Man 2019;29:100781. https://doi.org/10.1016/j.addma.2019.100781.
[19] https://solidarites-sante.gouv.fr/IMG/pdf/Tableau_Toxicite_des_metaux_et_des_metalloides_sous_leurs_differentes_formes_chimiques_.pdf.
[20] Simchi A, Pohl H. Effects of laser sintering processing parameters on the microstructure and densification of iron powder. Mater Sci Eng, A 2003;359(1–2):119–28. https://doi.org/10.1016/S0921-5093(03)00341-1.
[21] Simchi A. The role of particle size on the laser sintering of iron powder. Metall Mater Trans B 2004;35B:937–48. https://doi.org/10.1007/s11663-004-0088-3.
[22] Kruth JP, Froyen L, Van Vaerenbergh J, Mercelis P, Rombouts M, Lauwers B. Selective laser melting of iron-based powder. J Mater Process Technol 2004;149:616–22. https://doi:10.1016/j.jmatprotec.2003.11.051.
[23] Song B, Dong S, Deng S, Liao H, Coddet Ch. Microstructure and tensile properties of iron parts fabricated by selective laser melting. Opt Laser Technol 2014;56:451–60. https://doi.org/10.1016/j.optlastec.2013.09.017.
[24] Letenneur M, Brailovski V, Kreitcberg A, Paserin V, Bailon-Poujol Ian. Laser powder bed fusion of water-atomized iron-based powders: process optimization. J Manuf Mater Process 2017;1(23):1–17. https://www.mdpi.com/2504-4494/1/2/23.
[25] Palousek D, Pantelejev L, Zikmund T, Koutny D. Processing of nearly pure iron using 400w selective laser melting – initial study. MM Sci J 2017:1738–43. https://doi.org/10.17973/MMSJ.2017_02_2016184. 01.
[26] Pasquet I, Baco-Carles V, Chamelot P, Gibilaro M, Massot L, Tailhades Ph. A multimaterial based on metallic copper and spinel oxide made by powder bed laser fusion: a new nanostructured material for inert anode dedicated to aluminum electrolysis. J Mater Process Technol 2020;278:116452. https://doi.org/10.1016/j.jmatprotec.2019.116452.
[27] Valdez-Nava Z, Guillemet-Fritsch S, Tenailleau Ch, Lebey T, Durand B, Chane-Ching JY. Colossal dielectric permittivity of $BaTiO_3$-based nanocrystalline ceramics sintered by spark plasma sintering. J of Electroceram 2009;22(1–3):238–44. https://doi.org/10.1007/s10832-007-9396-8.
[28] Syed K, Xu M, Ohtaki KK, Kok D, Karandikar KK, Graeve OA, et al. Correlations of grain boundary segregation to sintering techniques in a three-phase ceramic. Materialia 2020;14:100890. https://doi.org/10.1016/j.mtla.2020.100890.